Spectrum of Engineering Sciences
ISSN (e) 3007-3138 (p) 3007-312X Volume 4, Issue 1, 2026

FAGONIA-SYNTHESIZED TITANIUM DIOXIDE NANOSTRUCTURES FOR DYE- SENSITIZED SOLAR CELL APPLICATION

Muhammad Waqar Ejaz[1], Atif khalil[2], Salman Khan[3], Faisal Munir[4], Dr Gul Naz[*5]

[1,3]*Research Scholar, Institute of Physics, Islamia University Bahawalpur Punjab Pakistan*
[2]*Research Scholar, M.Phil Quaid-I-Azam University Islamabad, Pakistan.*
[4]*Department School of Science XATU, Xi'an Technological University Weiyang Campus Xi'an shaaxi province China.*
[*5]*Assistant Professor, Institute of Physics Islamia University Bahawalpur Punjab, Pakistan.*

[1]waqarqureshi414@gmail.com, [2]atif.22311011@chem.qau.edu.pk, [3]khanjii806@gmail.com, [4]fmunir753@gmail.com, [*5]gul.naz@iub.edu.pk

DOI: https://doi.org/10.5281/zenodo.18322891

Keywords
Green synthesis; Titanium dioxide nanoparticles; Fagonia indica; Dye-sensitized solar cells; Nanostructures; Photovoltaic performance.

Article History
Received: 24 November 2025
Accepted: 05 January 2026
Published: 21 January 2026

Corresponding Author: *
Dr Gul Naz

Abstract
Green synthesis of semiconductor nanomaterials has emerged as a sustainable alternative to conventional chemical routes due to its environmental compatibility, low cost, and simplicity. In this study, titanium dioxide (TiO_2) nanostructures were successfully synthesized using Fagonia indica leaf extract as a natural reducing and stabilizing agent. Size, FTIR, UV-Vis Spectroscopy, and SEM were all used to characterize the produced Fg-TiO2 NPs. FTIR analysis, by revealing distinct absorption peaks in various locations, proves that leaf extract contributes to the production of Fg-TiO2 NPs. Using a UV-Vis spectrophotometer set at 273 nm and bandgaps of 3.15 eV and 3.26 eV, we verified the excitation of the green-synthesized Fg-TiO2 NPs. When the growth of Fg-TiO2 nanoparticles on FTO substrate become scattered. A DSSC based on film B, has power conversion efficiency of 4.45%, which is 24% greater than the power conversion efficiency of film A. Also increase in other parameters of DSSC just like open circuit voltage, fill factor and current density. The values for fill factor, open circuit voltage and current density in Film A, are 0.62V, 0.59 and 6.9 mA/cm2 respectively. The values for fill factor, open circuit voltage and current density in Film B, are 0.69V, 0.63 and 8.04 mA/cm2 respectively.

INTRODUCTION

The rapid growth of global energy demand and the environmental concerns associated with fossil fuel consumption have intensified research into renewable and sustainable energy technologies. Among various renewable energy sources, solar energy has gained considerable attention due to its abundance, cleanliness, and long-term viability [1]. However, the development of efficient, low-cost, and environmentally friendly solar energy conversion devices remains a major scientific and technological challenge. Dye- sensitized solar cells (DSSCs), introduced by O'Regan and Grätzel, represent a promising third-generation photovoltaic technology owing to their low fabrication cost, simple processing techniques, and good performance under diffuse light conditions [2].

Nanoscience and technology are frequently the results of human dreams and creativity. Nanotechnology is the study and manipulation of matter at dimensions ranging from 1 to
100 nm, where special phenomena allow for novel applications [3]. Although nanoparticles have always

existed, their exposure increased dramatically during the industrial revolution. Nanomaterials research is not brand-new. “Richard Zsigmondy”, the 1925 winner of the Nobel Prize in chemistry, was the one who initially coined the term "nanometer" He was the first to use the microscope to measure the size of particles like gold colloids, and he also invented the term nanometer specifically to describe particle size. Richard Feynman was the inventor of modern nanotechnology. Nanotechnology is the ability to manage and restructure matter at the atomic and molecular levels between 1 and 100 nm by taking advantage of the unique properties and phenomena that exist there as opposed to those that are connected to different atoms or molecules or unpackaged behavior [4]. A material is called a nanomaterial if it has one measurement in the nanoscale range of 1 to 100nm. Nanomaterials have emerged as an intriguing class of materials with a wide range of uses. Nanotechnology boosts productivity and long-term consistency while remaining inexpensive, allowing for the production of low-cost goods [5]. Materials with all of their dimensions at the nanoscale are known as zero-dimensional nanomaterials, which never exceeds from 100 nm [6].

The future success of this new technology depends on the synthesis of nanomaterials, and in theory, there are two primary kinds of nanomaterial synthesis methods: both top-down and bottom-up strategies [7]. Nanoparticles' chemical characteristics are crucial. Oxidation, toxicity, antibacterial, and disinfectant are some of the chemical characteristics of nanomaterials. The size of nanoparticles also affects their chemical characteristics and alters in terms of size. The smaller nanomaterials have more atoms on them as their surface area is greater than that of bulk materials [8]. As a result, nanomaterials are more reactive. The following are a few examples of chemical properties when compared to other bulk materials:

Surface properties of nanomaterials are influenced by the availability of up to 50% of atoms. Nanomaterials have more atoms on their surface than large structures, which increases their average energy [9]. For instance, compared to bulk materials, nanoparticles exhibit higher catalytic activity. Per atom, the nanomaterials exhibit more chemical activity. Unveiled surface Comparing bulk materials to nanomaterials, the catalytic activity diminishes. The increased chemical activity is caused by the many atoms that are exposed to the exterior [10]. Roy, Komarneni, and their fellow coined the term "nanocomposites" for the first time in 1982-1983. Nanocomposites are bifunctional materials with a huge number of individual phase domains and a small number of phases with nanoscale dimensions [11]. Nowadays, nanocomposites have emerged as advantageous options for overcoming the limitations of various engineering materials. They are referred to as the materials of the twenty-first century because they have design characteristics and property combinations that traditional composites do not have. Dispersion phase materials or dispersed phase materials can be used to classify nanocomposites. Through this expanding field, it is now possible to create new materials with advanced properties using novel synthetic methods.

2. LITERATURE REVIEW

In 2017, Ullattil et al., explains a rapid and efficient synthesis of mesoporous anatase TiO2 nanoparticles for use in DSSCs was achieved using a microwave method. The approach involved applying low microwave power intensities (301 and 601 W) for 5 minutes of irradiation. Characterization techniques analysis long-established the nanocrystalline anatase nature of the synthesized nanoparticles, with high surface area up to 210 m^2/g. These nanoparticles exhibited excellent performance as the working electrode in DSSCs, achieving an efficiency of 6.6% under 100% sunlight illumination and demonstrating a 55% IPCE (incident photon-to-current efficiency) [16]. In 2019, Maurya et al., reported TiO2 NPs were successfully synthesized from Titanium (IV) butoxide solution using an environmentally friendly approach involving Bixa orellana seed extract. This method offers a low cost and eco-friendly alternate to conventional chemical and physical methods, which often involve toxic solvents and high energy consumption [16]. In 2018, Sharma et al., introduces an innovative and environmentally friendly approach for synthesizing TiO2 NPs using the green/alga/Chlorella/pyrenoidosa. These nanoparticles were then combined with GO to

create a TiO2-GO [29]. In 2016, Mohan Kumar et al., introduces a straightforward and environmentally friendly approach to synthesizing Sulphur/doped TiO2 MSs using a direct self-assembly process. Through ultrasonication of TiOSO4 in aqueous media followed by refluxing, S-TMS structures are formed, where sulphate ions fashioned during the reaction act as a cause for sulphur doping. Despite the acidic pH conditions, the increased availability of sulphate ions favors the development of a pure anatase phase, as confirmed by XRD, while the resulting S-TMS structures with microrods containing self-assembled nanorods were verified using microscopy techniques [30]. In 2021, Isnaeni et al., shows green synthesis method was employed to produce TiO2 NPs by hydrolyzing TiCl3 using mango/peel extract as the reducing agent. The reaction occurred in an aqueous solution under acidic situations at 80 °C for 24 hours. Through the manipulation of the extract-to-TiCl3 ratio, the crystal structure of the TiO2 NPs were controlled, with an increase in the extract content leading to a decrease in product characteristics and phase composition. Specifically, employing 5 mg of extract resulted in 100% rice-grain-like rutile NPs (28 nm), while using 15 mg yielded 100% anatase spherical nanoparticles (~17 nm) [13].

In 2021, Aslam et al., processed nanoparticles (NPs) possess valuable properties for diverse applications, but traditional production methods often pose health and environmental risks [31]. In 2022, Roy et al., explains the increasing interest in nanoscale materials stems from their unique properties in various domains such as chemistry, physics, optics, and mechanics. Titanium dioxide (TiO2) stands out due to its non-toxic nature, corrosion resistance, and thermal stability, leading to applications like photocatalysis, solar cells, self/cleaning surfaces, and wastewater treatment [32]. In 2021, Narayanan et al., investigates the potential of using the aqueous leaf extract of Pouteria campechiana to synthesize TiO2 NPs and assesses their larvicidal-and-pupicidal actions against Aedes aegypti mosquitoes. Results revealed successful TiO2 NP synthesis through analysis, displaying a distinct peak at 325 nm. SEM analysis showcased spherical TiO2 NPs, while XRD revealed five distinct diffractions characteristic of TiO2 [17]. In2020, Irshad et al., compares the production of TiO2 NPs using green methods with plant extracts of Trianthema portulacastrum and Chenopodium quinoa, and a conventional sol-gel method (T1). The synthesized TiO2 NPs were characterized using advanced techniques. The antifungal activity of these TiO2-NPs was evaluated against Ustilago tritici, a toxic plant pathogen causing wheat rust. Results demonstrated successful TiO2-NP synthesis with all methods, but the green approach, particularly using Chenopodium quinoa extract, exhibited the most potent antifungal activity, suggesting its potential for large-scale and environmentally friendly TiO2-NP synthesis with versatile applications [14]. In 2022, Sunny et al., reported biosynthesized nanoparticles have gained significant attention for their diverse applications, with plants being a prominent source for green synthesis due to their eco-friendly nature. TiO2 nanoparticles are extensively used in consumer products and nanotechnology, and this review provides insights into their green synthesis, characterization, and current applications [33]. In 2018, Boro et al., focuses on DSSCs, a promising third-generation-photovoltaic technology known for its low cost, stability, non- toxic manufacturing, and design flexibility. The review delves into advanced methods and research trends involving the combination of ZnO with TiO2 in various nanostructures. Bridging the efficiency gap among conventional silicon solar cells and DSSCs is a key research area, driving the quest for efficient photoanodes. Engineered nanostructured metal oxide photoanodes, particularly TiO2/ZnO nanocomposites in diverse structures like nanodonuts, nanoflowers, and 3D hierarchical heterostructures, enhance DSSC performance with improved electron transfer rates, charge recombination reduction, and larger surface areas. Their efficiency parameters fall within ranges that highlight their potential for enhancing DSSC performance [12]. In 2021, Irshad et al., shows nanotechnology's broad applications have generated global interest, with titanium dioxide (TiO2) nanoparticles being extensively used and synthesized through various methods. Green synthesis offers a nontoxic, low cost, and environmentally friendly approach. This review compiles data on various synthesis techniques, emphasizing the superiority of

green methods due to reduced precursor usage, time efficiency, and energy conservation. The review discusses plant, microorganism, and biological derivative sources employed in TiO2 NP synthesis, highlighting their applications in water treatment and plant physiology enhancement under abiotic stress conditions. The review also outlines future directions for enhancing TiO2 NP production and its reliable applications [15]. In 2018, Subhapriya et al., shows the biosynthesis of nanoparticles has gained significant attention for its environmentally friendly, cost-effective, and renewable approach. This study focused on the biosynthesis of TiO2 NPs involving the aqueous leaf extract "Trigonella/foenum/graecum". Characterization techniques were employed to analyze the synthesized TiO2 NPs. The X-ray diffraction confirmed the presence of TF-TiO2 NPs, with peaks at 25.28 corresponding to the anatase phase. HR-SEM observations revealed spherical nanoparticles with sizes ranging from 20 to 90 nm, while antimicrobial assays using the Kirby-Bauer method demonstrated significant antimicrobial activity of the TF- TiO2 NPs against all tested microorganisms [40].

3. MATERIALS AND METHODS

This research was carried out in response to the growing need for environmentally friendly technologies. All chemicals used in this study were of analytical grade and were utilized without further purification. Titanium dioxide precursor materials, tin chloride (SnCl2), ethanol, acetone, and other reagents were obtained from standard commercial suppliers. Fagonia indica leaves were used as a biological reducing and stabilizing agent. Fluorine-doped tin oxide (FTO) glass substrates were employed for photoanode fabrication. Double-distilled water was used throughout the experimental procedures.

The data are shown in the table that can be seen below.

3.1 Required Chemicals

The compounds listed below are those employed in the TiO2 production process.

Table 2.1: Chemical required for the synthesis of Fg-TiO2 NPs

Sr.no	Name of Chemical	Formula	Brand
	Titanium Dioxide Powder	Titanium Dioxide Powder	Sigma Aldrich
02	Tin Chloride	SnCl2	Sigma Aldrich
03	Ethanol	CH3CH2OH	
04	*Fogonia Indica* Powder		Sigma Aldrich
05	Acetone	CH3COCH3	
06	double distilled water	H2O	

3.1.1 Apparatus

For the experimental work of TiO2 NPs, the following apparatus is used:

1. Electronic Balance
2. Magnetic Stirring
3. Spatula
4. Beakers
5. Dropper
6. Micro-Pipettes
7. Eppendorf Tubes
8. Centrifuge Machine
9. Thermometer
10. Whatman filter papers
11. Magnetic Stirrers
12. Autoclave
13. Oven
14. Crucible Cups

Pyre brand-made glassware, including the conical flask, funnel, beaker, and measuring cylinder. The materials were covered with a silicon coating to prevent contaminants from seeping in. The reagent sucker is where you put the exact quantity. The stirring was done using a magnetic stirrer. The temperature was monitored and kept steady with the

use of a thermometer. The NPs are ground into a powder using a mortar and pestle.

3.1.2 Plant collection

The part of the plant known as the Fogonia responsible for its botanical characteristics was gathered from the wall surrounding Bahawalpur. The obtained plant specimen was analyzed to determine its species.

3.1.3 Preparation of plant Extract

The powdered form of Fogonia Indica is first measured by weight. Fill a beaker with distilled water and add the powder. For 10 minutes, use a hot plate to maintain a temperature of 100 degrees Celsius. Let it cool, then strain it using Whatman filter paper.

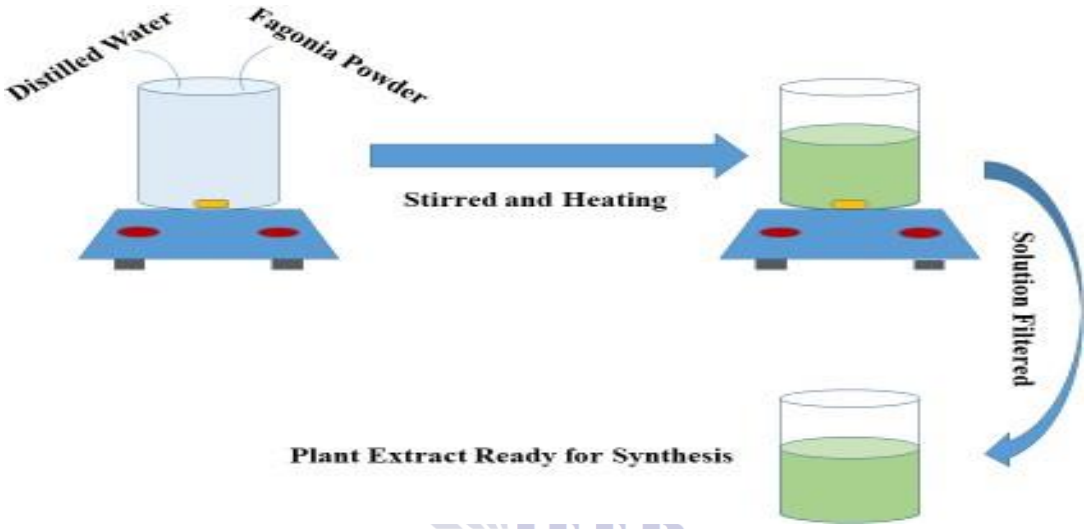

Figure 2.1: Schematic Diagram of preparation of plant extract

3.2 Green synthesis of Titanium Dioxide Nanoparticle

TiO2 green NPs were synthesized by creating a powdered TiO2 solution. We prepare 0.08 M, and 0.16 M solutions, each with a unique concentration. A plant extract of Fogonia Indica, measured to be 60 ml, is added to 300 ml of TiO2 powder solution in a beaker. The mixture is stirred constantly for 4 hours to produce a range of molarity samples.

Figure 2.2: Schematic Diagram of preparation of Titanium oxide

Table 2.2: Shows the quantity used during each reaction.

Sr. No	Sample name	The molarity of TiO2 used	The volume of TiO2 used	Importance of Plant Extract used
1	A	0.08 M	300 ml	60 ml
2	B	0.16 M	300 ml	60 ml

The produced nanoparticles remain in the dark for 24 hours after being stirred for 4 hours continuously. Protect the beaker from contamination by rapping it with a silicon sheet to absorb any lingering impurities. After the nanoparticles have dried, they are ground into a powder using a mortal pistal. The next step is to characterize this powder.

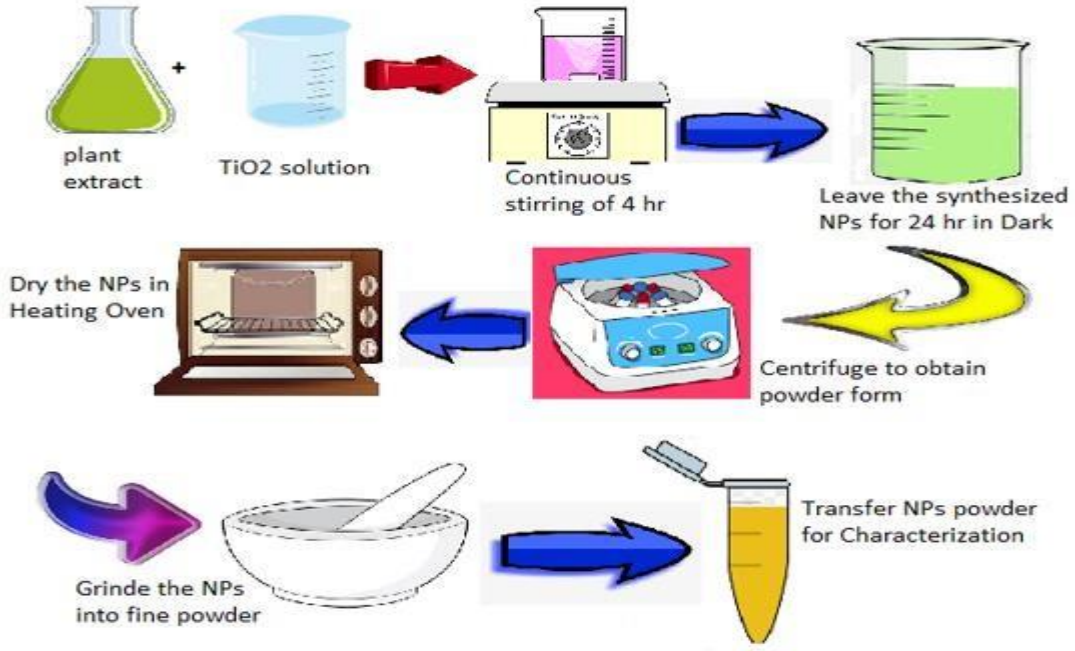

Figure 2.3: Schematic Diagram of Green Synthesis of Titanium Dioxide Nanoparticles

3.3 Characterization

3.3.1 Ultraviolet-Visible Spectroscopy

UV-visible spectroscopy is one of the simplest, economical and efficient employed techniques to characterize quantitatively inorganic as well as organic nano sized materials with a length not less than 2 nm [18]. UV-Visible (UV-vis) spectroscopy is used to study the optical properties of materials in which change in absorbance is taken as a function of wavelength. By absorbing UV and visible light molecules holding non-binding electrons gets excited to higher antibonding molecular orbits. UV-Vis spectroscopy diverges from IR spectroscopy, however, in IR spectroscopy, molecules undergo vibrational transitions in the IR region. The intensity of light from the source is firstly measured by the detector and again same light is measured after being transmitted from the sample. The difference between light from the source and transmitted light from 27 the sample gives absorbance of that sample. Finally, absorbance versus wavelength is plotted to analyze the optical properties [19].

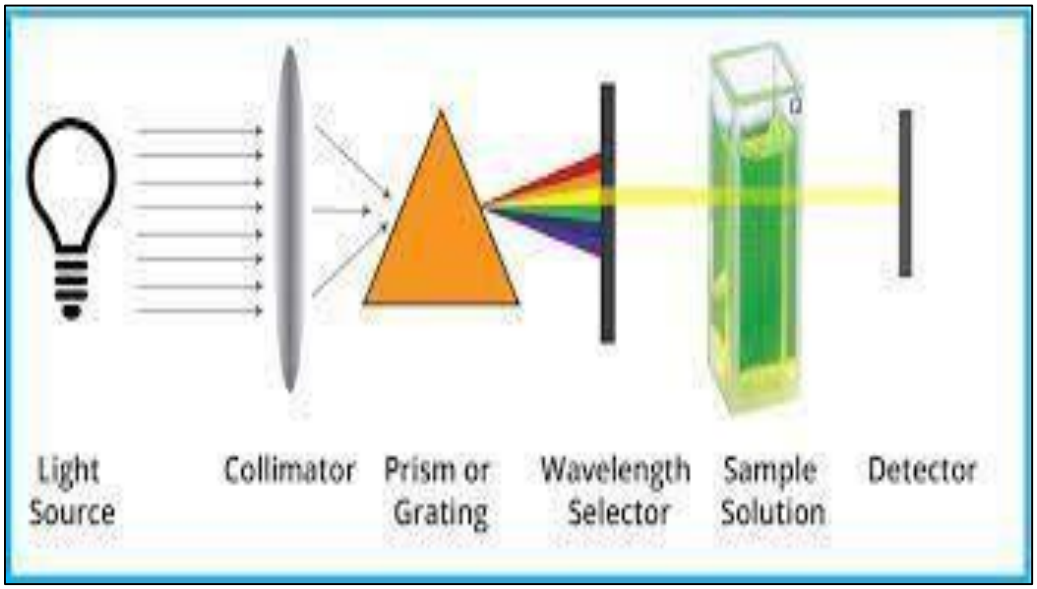

Figure 2.4: Process flow diagram for UV-Visible spectroscopy [76].

The Beer-Lambert equation is a mathematical formula that relates an absorbers concentration, absorbance and path length. It's stated as;

$(x) = I_o 10 - ax$

Where;

I(x) = Later, as light passes through the thickness x, its intensity decreases.

I_o = Original light intensity and the proportionality constant

X-Ray Diffraction Method

3.3.1.1 Production of x-ray

In order to produce X-rays, thermal electrons from a tungsten filament in vacuum are accelerated towards and eventually collide with a metal anode with a high potential. The retardation of these electrons as they penetrate matter is the most crucial mechanism for the production of X-rays. According to Maxwellian theory, a continuous spectrum is generated for each variation in the velocity of a charged particle [20].

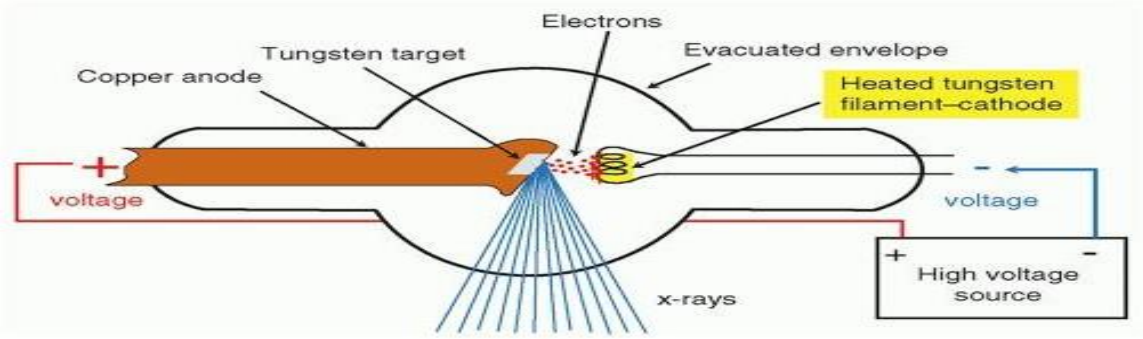

Figure 2.5: X-ray tube

3.3.1.2 Introduction of X-ray Diffraction Method

XRD has been used extensively to evaluate the structural and microstructural features of these materials. It can be used to analyze a variety of thin-film properties for the manufacturing of semiconductors. These are some of them:

- The proportion of crystallinity in nominally amorphous films is measured.

- The composition of crystalline material is measured.
- Crystalline material's grain size is determined.
- Evaluation of the crystalline material's stress.
- A polycrystalline material's crystallographic texture, or the distribution of crystallite orientations, is measured.

3.3.1.3 Principle of x-ray diffraction

A regular arrangement of atoms is known as crystalline material. When X-rays collide with crystalline material, they can interact in a number of different ways. So, elastic scattering or Thompson scattering occurs when the energy of an entering and exiting photon is the same. Constructive or destructive interference occurs when radiation is emitted. Peaks from constructive-interference diffraction are collected and analyzed. In contrast to destructive interference, constructive-interference follows Bragg's law.

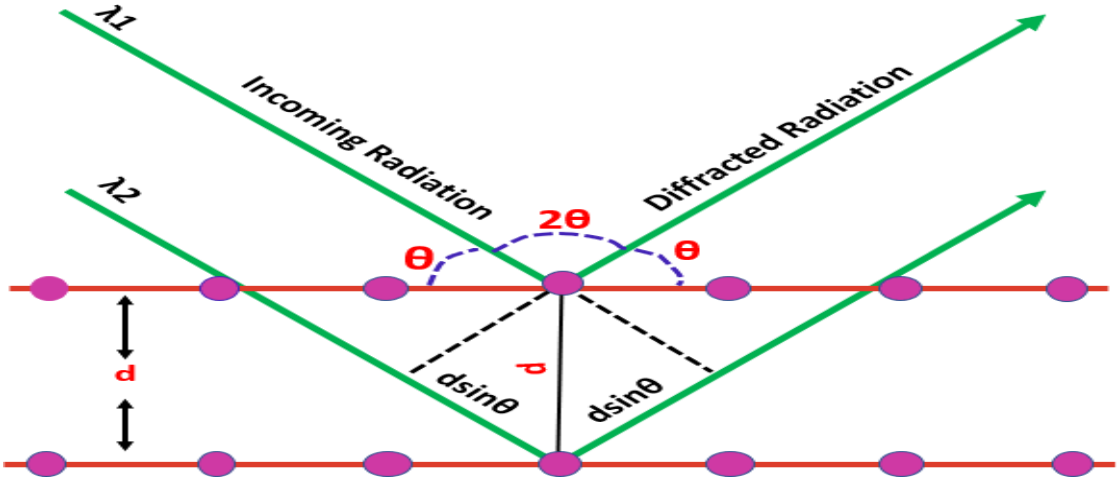

Figure 2.6: Geometrical representation of Bragg's law.

3.3.2 Fourier-Transform Infrared Spectroscopy

FT-IR analysis uses infrared light to scan samples to detect their organic, inorganic, and polymeric compositions. A sample is passed through 100-10,000 cm-1 infrared light, some of which is absorbed and part of which passes through. The absorbed radiation is converted to vibratory or rotational energy by the sample. As a result, the detected signal exhibits a spectrum ranging from 4000 to 400 cm-1, that indicating the samples' molecular fingerprint. Fourier Transform Infrared has become a useful technique for chemical identification because every component has its unique identity [21].

3.3.2.1 Basic Principle of FT-IR

Infrared radiation strikes a sample, which absorbs light and induces a number of vibrational modes. The frequency of the absorbed radiation is recorded in wave numbers between 600 to 4000cm-1, and the absorption frequency is directly proportional to the nature of bonds present in the molecule. The FTIR spectrum is measured as wave number because energy and frequency are directly related to wave number. To reduce air and water vapor contamination peaks, the environment is recorded before the sample analysis. The ratio of the environment and sample spectra is directly proportional to the absorption spectrum of the sample. The absorption spectra of the sample molecule revealed the different bond vibrations. As a result, this method makes it simple to identify the functional group in a molecule.

3.3.2.2 Instrumentation

Detector, amplifier, an IR source, interferometer, testing chamber, and computer are all part of a conventional FTIR spectrometer. As the sample travels through the interferometer and eventually falls on the detector, it is exposed to radiation from the light source. The interferogram is finally transformed into a spectrum using the fast Fourier transform procedure[22-25].

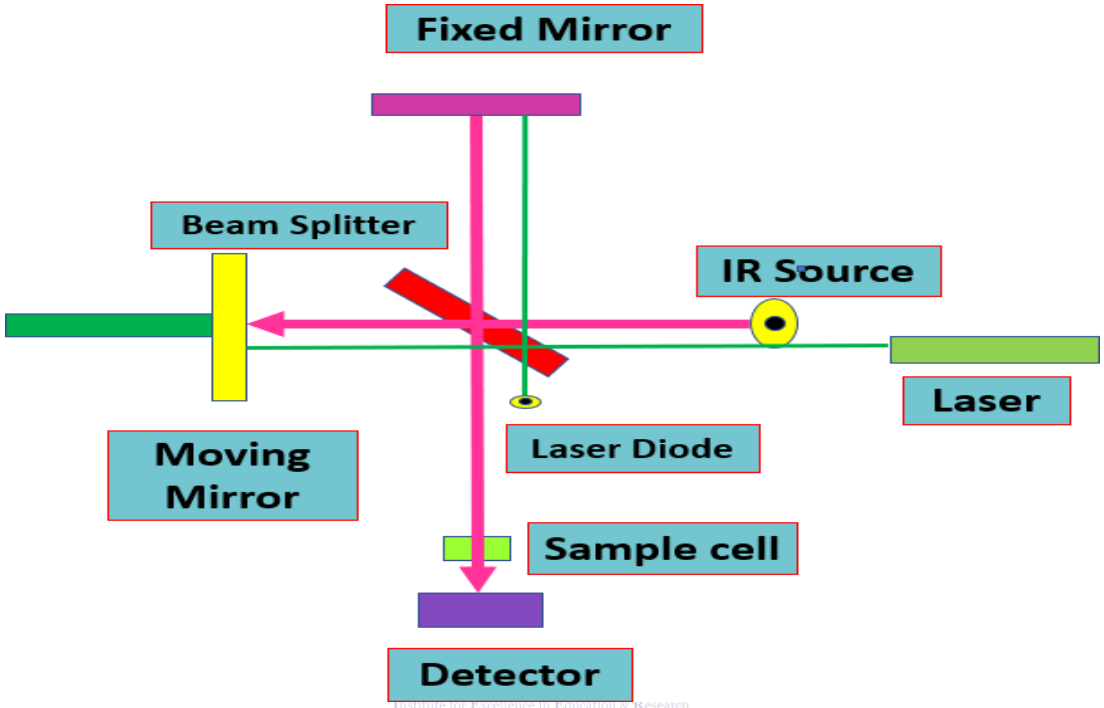

Figure 2.7: Schematic diagram of an FTIR spectrometer.

3.3.2.3 Interferometer

The optical device known as an interferometer or interference meter is a major component of the FTIR instrument as shown in figure. In the interferometer, light from an infrared source was separated into two light beams. The variation in distance travelled by the 2 light rays is known as the Optical Path-difference. When the first path is 0.04m long and the second path is 0.1m long, then optical path difference is 0.04 - 0.1m = 6m. The condition zero path difference occurs if the beam splitter is at the same distance between the moving and fixed mirrors and separation between the two light beams is the same in the interferometer. So, it is the most popular form of interferometer used in FTIR nowadays [26, 27].

3.3.2.4 Sample-Holders in FTIR

FTIR spectrometer uses a variety of sample containers, as described below.

3.3.2.5 Universal Sample Holder

The techniques to allow placing potassium Bromide pellets, salted plates, films, and many other samples is called spring-loaded technique. The holder's aperture is 10- 20mm, and it allows for precise sample holding.

3.3.2.6 Heavy-Duty Magnetic Film Holder

Polymer materials are used to make such kind of holder. This type of holder has a 20 mm hole and a large steel plate.

3.3.2.7 Magnetic Film OR Pallet Holder

Potassium Bromide pellets and thin polymer films are placed in this kind of container. It is made up

of an elastic magnetic strip and a steel plate. It is used to hold thin polymer films with a diameter of 0.5 mm and potassium Bromide pellets with a thickness of 13 mm.

3.3.2.8 4 Press-on demountable cell holders

This type of holder is used to examine into mull and smear samples. There are two sizes available: 25 mm and 38 mm. Each holder has a mounting plate and pressure cap.

3.3.2.9 5 Single Pellet holder

Due to the 7 mm pellets, this type of sample holding is more suitable than the dual- pellet holder. This technology had been used in the two types of pressers

- Pike Technologies Pallet Press
- Pixie Hydraulic Pallet Press.

3.3.2.10 Dual-Pellet holder

It has 1mm, 3mm, and 7 mm Potassium Bromide pellet semicircular supports with holes, which can be used for pellets of the indicated size. Low-cost sample holders are pike Technologies Sampling Cards. They were used to evaluate polymers, films, and Potassium Bromide pellets (13 mm).

3.3.2.11 Bolt-Press and Gas Cell Holders

Large sample and salt plate holders are placed in these holders. These holders are organized into three different styles. Each has a supporting rod with various sized fasteners that can be quickly separated. [34].

RESULTS AND DISCUSSION

4.1 UV-Visible Spectroscopy Analysis

Fg-TiO2 NPs, generated in a green synthesis, are characterized by ultraviolet and visible spectroscopy. UV-Vis spectroscopy is used to assess produced samples' electronic structure and optical characteristics. Therefore, it was the primary approach to monitor the reduction of pure Fg-TiO2 NPs after diluting the solution. Nanoparticles' ability to absorb light is quantified by analyzing their visible absorption spectra. Figure4.1 shows that the as-synthesized Fg-TiO2 NPs exhibited UV-Visible absorption spectra at 224 nm and 273 nm [35]. With a direct energy band gap, the optical energy band of a metal oxide may be calculated as follows: Let k be a constant; let is the absorption coefficient; let Eg be the energy band gap; and let n be 1; this gives us the optical energy band. Using the tauc plot of (hv)2 against photon energy, the energy band gap may be calculated (hv). When n is 1, the band gap is shown explicitly by the point where the tangent to the tauc plot intersects. Preparation of Fg-TiO2 NPs yields a band gap of 3.15 eV and 3.26 eV, close to 3.2 eV, the same as bulk Fg-TiO2 NPs [36]

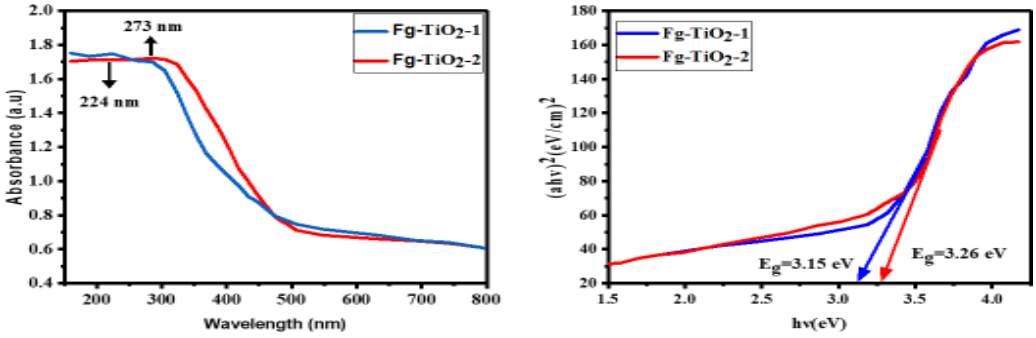

Figure 1.1: UV-Visible spectroscopy of Fg-TiO2 NPs showing band gap and absorption peaks.

4.2 X-Ray Diffraction Analysis

According to the XRD pattern, the produced nanoparticles are of Fg-TiO2 NPs. Miller indices of (101), (110), (103), (004), (112), (200), (105) and (211) for the Titanium dioxide lattice planes in the XRD patterns for the pure crystalline metallic phase Fg-TiO2 NPs suggest a small degree of variation for the tetragonal structure, which is observed at the

diffraction peaks of the synthesized angles of TiO2 NPs are around 24.78º, 28.30º, 34.80º, 36.61º, 38.09º, 47.16º, 58.46º and 59.61º. The particle size distribution of Fg- TiO2 NPs is responsible for the modest shifting (concerning JCPDS No. 21-1272 and 21- 1276). The rate of crystallinity is increased by showing an increase in the diffraction peaks [37].

4.3 Calculation of the Average Lattice Size of TiO2 NPs

The prepared samples lattice size (D) may be determined using the Debye-Scherrer equation, which has the following numerical form

Where,

$D = 0.9 \times \lambda \beta COS\theta$

λ = is the X-ray wavelength used in the experiment.

β = maximum intensity at half width

θ = Bragg's angle

According to the Scherer formula, D has values of 41.6 nm and 42.47 nm Fg-TiO2 NPs respectively.

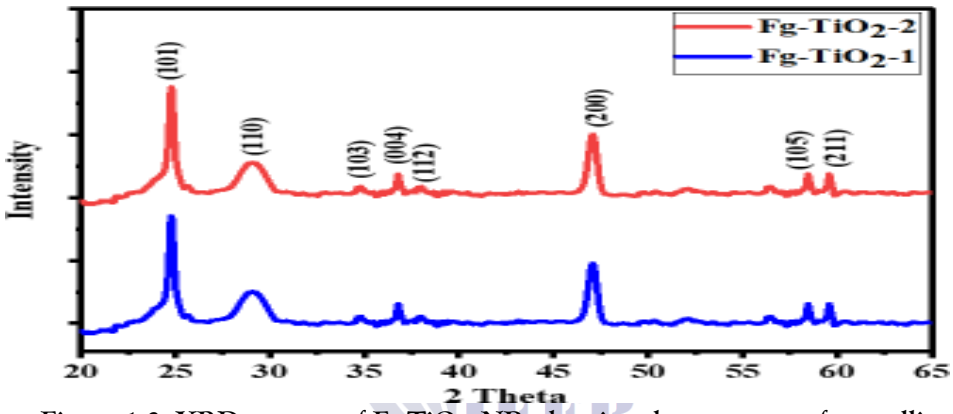

Figure 1.2: XRD pattern of Fg-TiO2 NPs showing the structure of crystallite

4.4 Scanning Electron Microscopic Analysis

To obtain accurate visual surface images of samples, is an essential approach. While acquired topography describes the surface characteristics of the target material, such as its texture, smoothness and roughness, morphology in SEM photographs specifies the shape and size of the object. Images of TiO2 nanoparticles by the molarity of Fg-TiO2 used as 0.08 M were taken using a scanning electron microscope (SEM). Fg-TiO2 (0.08 M) material is shown in Figure 4.3 using SEM images which shows that multifaceted cuboctahedral. The morphology of Fg-TiO2 (0.08 M) material which is constructed and agglomerates, and the synthesized nanoparticles were in nanometer scale with size of 122 nm.

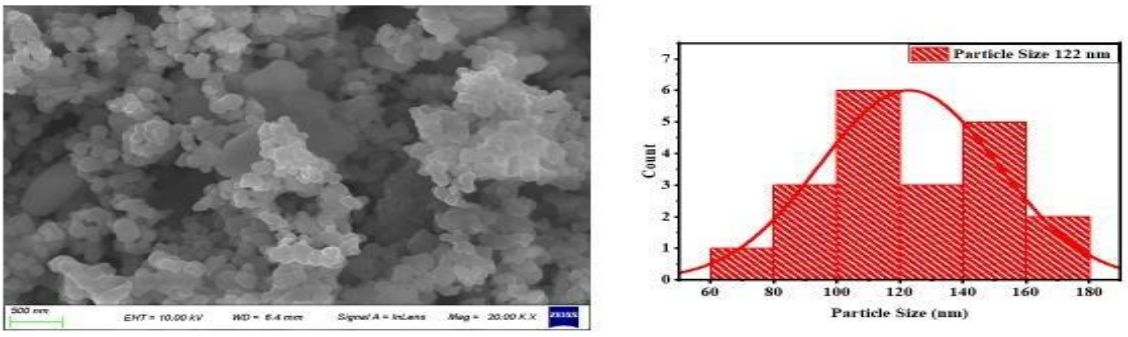

Figure 1.3: SEM images with Histogram of *Fg*-TiO2 (0.08 M) nanoparticles in nanometers.

4.5 Energy Dispersive X-Ray Analysis

Figure 4.4 shows the elemental mapping of the elements found in the prepared sample of Fg-TiO2 nanoparticles. The EDX results show that there is 75.35% oxygen due to the absorbed moisture and 24.65% titanium. From the elemental mapping, it is obvious that for Fg-TiO2 nanoparticles, there is dense distribution of titanium and oxygen in the sample. There is no other element detected in the EDX spectra which indicates that the prepared Fg-TiO2 nanoparticles are consistent with the XRD results. The weightage of titanium is 49.49% and oxygen is 50.51% [38].

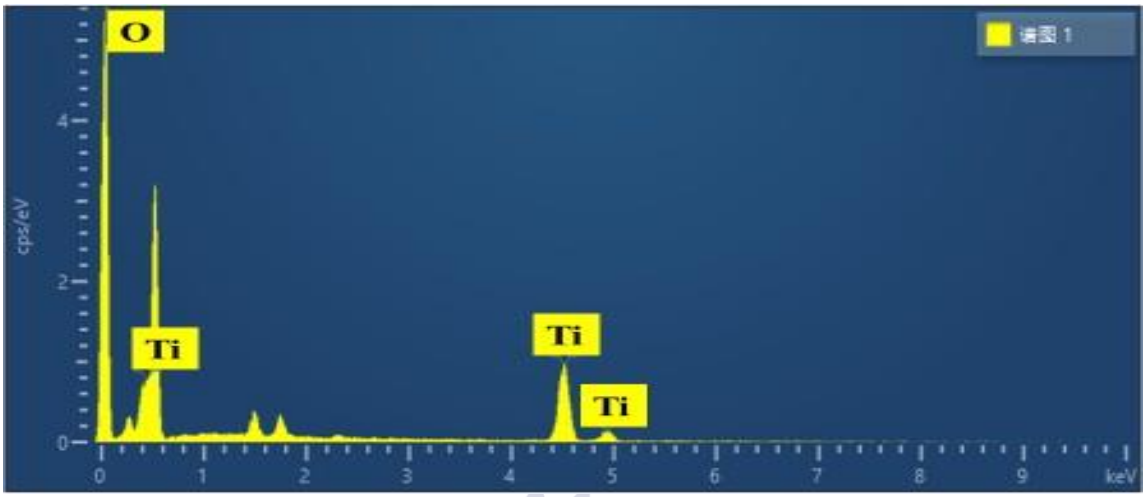

Figure 1.4: Energy dispersive X-ray spectra (EDX) of *Fg*-TiO2 nanoparticles.

4.6 FTIR Analysis

The presence of functional groups that were reasonable for reducing Fg-TiO2 NPs was analyzed using FTIR. Figure 4.5 shows the results of an FTIR spectrum analysis performed to verify the chemical compound formation between TiO2 NPs. Figure 4.5(a, b) displays the FTIR spectra of the Fogonia and Fg-TiO2 NPs samples, respectively. Band strengths at different wavelengths may be seen in the FTIR spectrum of produced Fg-TiO2 NPs. Figure 4.5(a) shows peaks between 983.08 and 1189.02 cm-1, a frequency range associated with stretching vibrations in the Ti-O-Ti bonds[100]. The C=O vibrations of carboxylic acid are indicated by the peak at 1074 cm-1 in frequency [28]. The peak at 1121 cm-1 is the extended vibration of the C-O group, which suggests tertiary alcohol[100]. The stretching of O-H bonds and hydrogen bonds is likely responsible for the appearance of a tiny absorption peak at 2922.70 cm-1. One of the stretching vibrations of Ti-O-Ti may be seen as a slight peak at 1450 cm-1. As shown in Figure 4. 5(b), the 540-785 cm-1 region of the IR spectra corresponds to the C-X (chloride) bond in a pure Fogonia, suggesting the presence of three peaks in this region. Alkenes and aromatic chemicals in Fogonia may be identified by a series of mountains in the 800-900 cm-1 part, representing the out-of-plane bending mode of vibrations. The second peak at 1170 cm-1 might be due to C-N (amines), C-X (fluoride), and C-O (alcohols, esters, ethers, anhydrides, carboxylic acid) bonds. Methyl (CH3) and methylene (CH 2) groups are present in Fogonia, which explains the plant's signature bending absorptions at 1373 cm-1 and 1462 cm-1. Fg-TiO2 NPs spectral analysis showed no evidence of these groups, indicating that the ligand was noncovalently bound to the nanoparticle's surface. An IR peak at about 1611 cm-1 in the Fogonia spectrum is more evidence of the existence of the C=C bond. Typically, it may be found between 1680 and 1600 cm-1 [24]. The two peaks show C-H stretching modes of vibrations in alkanes at 2914 cm-1 in (b) Fogonia and 2922 cm-1 in (a) Fg-TiO2 NPs.

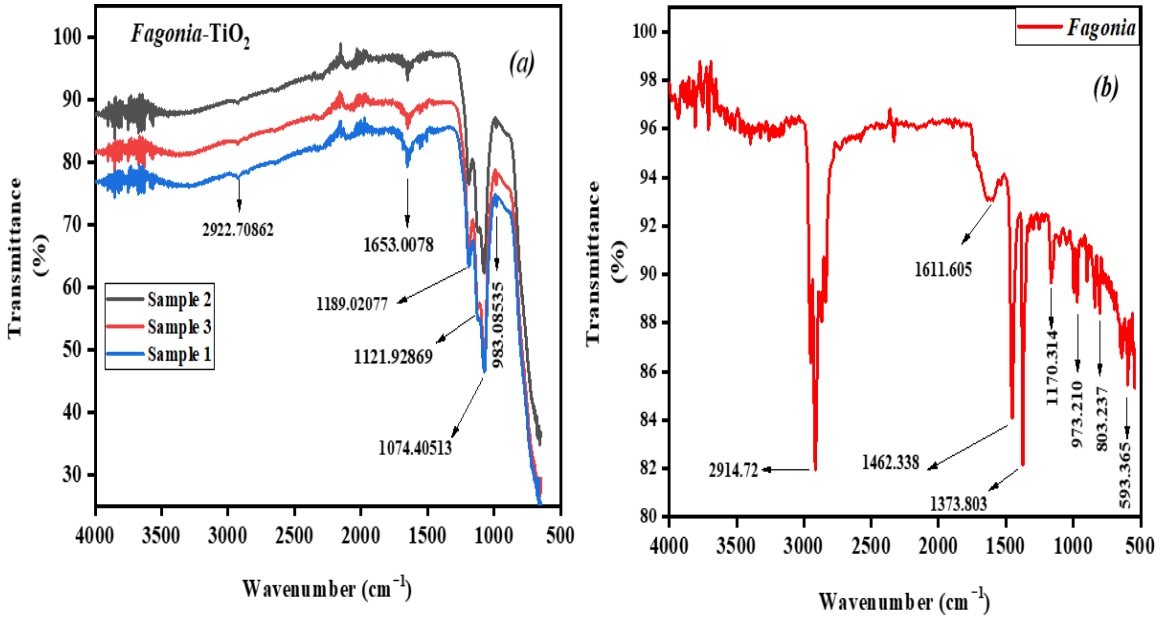

Figure 1.5: FTIR analysis of synthesized Fg-TiO2 NPs

Considering that no noticeable peaks in the region 3400-3500 cm-1 suggested an O-H bond, we may safely conclude that our samples were devoid of any traces of moisture. These peaks show that the synthesis of Fg-TiO2 NPs relies on the reducing molecules of Fogonia, which stabilize the particles by attaching functional groups like hydroxyl and secondary amines to their surfaces and reducing titanium ions [40]. The FTIR spectrum shows that the phenolic group of compounds, namely the more significant proportion of O-H stretching, plays a crucial role in the reduction process and the creation of Fg-TiO2 NPs nanoparticles. Moreover, the protein's amino acids and amide links keep the Fg-TiO2 NPs stable [17]. As a result, FTIR analysis confirmed the presence of several classes of phytochemicals, including phenol, alkanes, alkenes, alkynes, aldehydes, ketones, alcohols, esters, carboxylic acids, amines, and ethers that may be responsible for different pharmacological actions].

4.7 Performance of Solar Cell

Figure 4.6 shows the J-V characteristics of dye-sensitized solar cells assembled from sample A and B. The average measurements of parameters of photovoltaic were given in Table 4.2.The power conversion efficiency of dye-sensitized solar cells based on sample A (without PEI) is 3.7 % (Jsc = 6.93 mAcm−2), while the power conversion efficiency of dye-sensitized solar cells based on sample B (with PEI) is 4.45 % (Jsc =8.04 mAcm−2). The power conversion efficiency of sample B is higher than sample A, is 1.08%. The improvement in power conversation efficiency of 24% which was due to increase in length of TiO2 nanoparticles and also nanoparticles becomes uniform and aligned in one direction.

Table 1.1: Photovoltaic parameters for the DSSCs based on films A and B.

Cell Parameters	A (Without PEI)	B (With PEI)
JSC (mA/cm^2)	6.93 ± 0.01	8.04 ± 0.02
VOC (V)	0.62 ± 0.03	0.69 ± 0.02
FF	0.59 ± 0.04	0.63 ± 0.01
PCE (%)	3.37 ± 0.01	4.45 ± 0.02

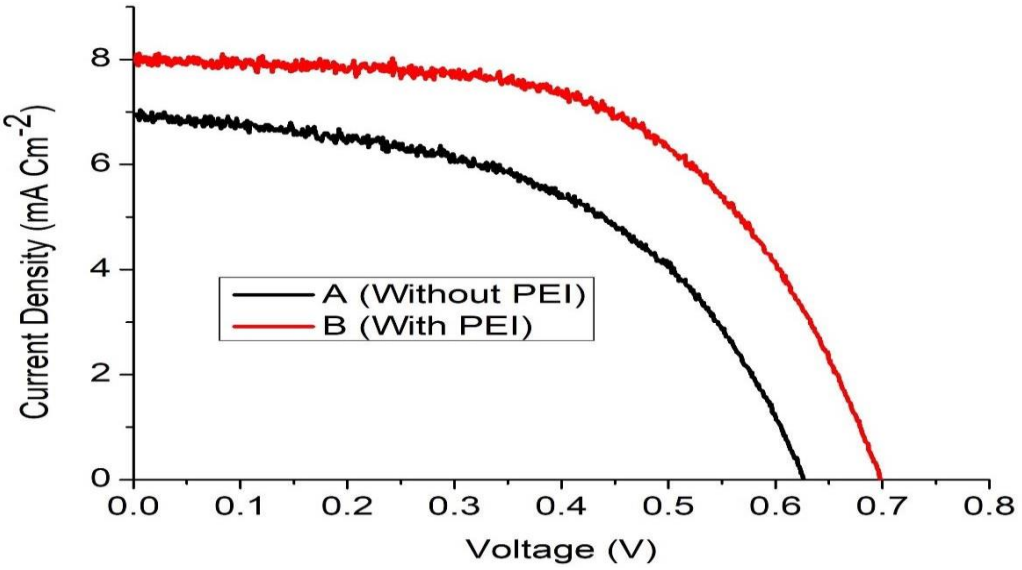

Figure 1.6: Current density–voltage characteristics of Film A and B.

5. CONCLUSION

In the present study, an eco-friendly and cost-effective green synthesis route was successfully employed for the preparation of titanium dioxide (TiO2) nanostructures using Fagonia indica leaf extract. The use of plant extract as a natural reducing and stabilizing agent eliminates the need for hazardous chemicals, making the synthesis process environmentally sustainable and economically viable.Fast and reliable synthesis of Fg- TiO2 NPs from a solution of Fogonia leaf extract has been shown. The UV-Vis spectrophotometer at 273 nm and bandgap of 3.15 eV and 3.26 eV validated the excitation of the green-produced Fg-TiO2 NPs. This study focuses on the biosynthesize of Fg-TiO2 NPs from a low-cost precursor, titanium dioxide, using an extract from the leaves of the Fogonia plant. Using leaf extract in a green chemistry process for synthesizing nanoparticles will boost economic viability and sustainable management. The investigation of plant systems as prospective nanofactories has piqued interest in the device fabrication of nanoparticles. A DSSC based on film B, has power conversion efficiency of 4.45%, which is 24% greater than the power conversion efficiency of film A. Also increase in other parameters of DSSC just like open circuit voltage, fill factor and current density. The values for open circuit voltage, fill factor and current density in Film A, are 0.62V, 0.59 and 6.9 mA/cm2 respectively. The values for fill factor, open circuit voltage and current density in Film B, are 0.63, 0.69V and 8.04 mA/cm2 respectively.

REFERENCES

Hulla, J., S. Sahu, and A. Hayes, Nanotechnology: History and future.
Human & experimental toxicology, 2015. 34(12): p. 1318-1321.
Pal, S.L., et al., Nanoparticle: An overview of preparation and characterization. Journal of applied pharmaceutical science, 2011(Issue):
p. 228-234.
Abid, N., et al., Synthesis of nanomaterials using various top-down and bottom-up approaches, influencing factors, advantages, and disadvantages: A review. Advances in Colloid and Interface Science, 2021: p. 102597.
Abd Ali, A., et al., Electrical Resistivity: Concept And Measurement. RESEARCH JOURNAL OF PHARMACEUTICAL BIOLOGICAL AND CHEMICAL SCIENCES, 2017. 8(2): p. 2038-2042.

Ray, U., What are the different types of nanoparticles, 2018.
Asha, A.B. and R. Narain, Nanomaterials properties, in Polymer science and nanotechnology2020, Elsevier. p. 343-359.
Wiechers, J.W. and N. Musee, Engineered inorganic nanoparticles and cosmetics: facts, issues, knowledge gaps and challenges. Journal of biomedical nanotechnology, 2010. 6(5): p. 408-431.
Teng, W.-Y., et al., Nanoparticles-doped guest-host liquid crystal displays. Optics letters, 2008. 33(15): p. 1663-1665.
Lu, Y.-C., et al., Platinum− gold nanoparticles: a highly active bifunctional electrocatalyst for rechargeable lithium− air batteries. Journal of the American Chemical Society, 2010. 132(35): p. 12170-12171.
Liu, X., et al., 3D hierarchically porous ZnO structures and their functionalization by Au nanoparticles for gas sensors. Journal of Materials Chemistry, 2011. 21(2): p. 349-356.
Mudshinge, S.R., et al., Nanoparticles: emerging carriers for drug delivery. Saudi pharmaceutical journal, 2011. 19(3): p. 129-141.
2Boro, B., et al., Nano-structured TiO2/ZnO nanocomposite for dye- sensitized solar cells application: A review. Renewable and Sustainable Energy Reviews, 2018. 81: p. 2264-2270.
Isnaeni, I.N., et al., Green synthesis of different TiO2 nanoparticle phases using mango-peel extract. Materials Letters, 2021. 294: p. 129792.
Irshad, M.A., et al., Synthesis and characterization of titanium dioxide nanoparticles by chemical and green methods and their antifungal activities against wheat rust. Chemosphere, 2020. 258: p. 127352.
Irshad, M.A., et al., Synthesis, characterization and advanced sustainable applications of titanium dioxide nanoparticles: A review. Ecotoxicol Environ Saf, 2021. 212: p. 111978.
Maurya, I.C., et al., Green synthesis of TiO2 nanoparticles using Bixa orellana seed extract and its application for solar cells. Solar Energy, 2019. 194: p. 952-958.
Narayanan, M., et al., Green synthesis and characterization of titanium dioxide nanoparticles using leaf extract of Pouteria campechiana and larvicidal and pupicidal activity on Aedes aegypti. Environ Res, 2021. 200: p. 111333.
Feldt, S., E. a. Gibson, E. Gabrielsson, L. Sun, G. Boschloo and A. Hagfeldt. J. Am. Chem. Soc, 2010. 132: p. 16714-16724.
Tsubomura, H., et al., Dye sensitised zinc oxide: aqueous electrolyte: platinum photocell. Nature, 1976. 261(5559): p. 402-403.
Leandri, V., et al., An organic hydrophilic dye for water-based dye- sensitized solar cells. Physical Chemistry Chemical Physics, 2014. 16(37): p. 19964-19971.
Yella, A., et al., Porphyrin-sensitized solar cells with cobalt (II/III)– based redox electrolyte exceed 12 percent efficiency. science, 2011. 334(6056): p. 629-634.
Mathew, S., et al., Dye-sensitized solar cells with 13% efficiency achieved through the molecular engineering of porphyrin sensitizers. Nature chemistry, 2014. 6(3): p. 242-247.
Yu, Z., Liquid redox electrolytes for dye-sensitized solar cells, 2012, KTH Royal Institute of Technology.
Blanchard, L.A., et al., Green processing using ionic liquids and CO2.
Nature, 1999. 399(6731): p. 28-29.
Agarkar, S., Dye sensitized solar cell: optimizing materials, methods and optoelectronic effects. 2014.
Kim, S.-S., J.-H. Yum, and Y.-E. Sung, Improved performance of a dye- sensitized solar cell using a TiO2/ZnO/Eosin Y electrode. Solar energy materials and solar cells, 2003. 79(4): p. 495-505.

Al-Juaid, F. and A. Merazga, Increasing dye-sensitized solar cell efficiency by ZnO spin-coating of the TiO 2 electrode: effect of ZnO amount. Energy and Power Engineering, 2013. 2013.

Ullattil, S.G. and P. Periyat, Microwave-power induced green synthesis of randomly oriented mesoporous anatase TiO 2 nanoparticles for efficient dye sensitized solar cells. Solar Energy, 2017. 147: p. 99-105.

Sharma, M., et al., TiO2-GO nanocomposite for photocatalysis and environmental applications: A green synthesis approach. Vacuum, 2018. 156: p. 434-439.

Mohan Kumar, K., et al., Green synthesis of S-doped rod shaped anatase TiO2 microstructures. Materials Letters, 2016. 183: p. 211-214.

Aslam, M., A.Z. Abdullah, and M. Rafatullah, Recent development in the green synthesis of titanium dioxide nanoparticles using plant-based biomolecules for environmental and antimicrobial applications. Journal of Industrial and Engineering Chemistry, 2021. 98: p. 1-16.

Roy, J., The synthesis and applications of TiO2 nanoparticles derived from phytochemical sources. Journal of Industrial and Engineering Chemistry, 2022. 106: p. 1-19.

Sunny, N.E., et al., Green synthesis of titanium dioxide nanoparticles using plant biomass and their applications- A review. Chemosphere, 2022. 300: p. 134612.

S, A. and S. M, [EMIM] BF4 ionic liquid-mediated synthesis of TiO2 nanoparticles using Vitex negundo Linn extract and its antibacterial activity. Journal of Molecular Liquids, 2016. 221: p. 986-992.

Abisharani, J.M., et al., Green synthesis of TiO2 Nanoparticles using Cucurbita pepo seeds extract. Materials Today: Proceedings, 2019. 14:
p. 302-307.

Thakur, B.K., A. Kumar, and D. Kumar, Green synthesis of titanium dioxide nanoparticles using Azadirachta indica leaf extract and evaluation of their antibacterial activity. South African Journal of Botany, 2019. 124: p. 223-227.

Nasrollahzadeh, M. and S.M. Sajadi, Synthesis and characterization of titanium dioxide nanoparticles using Euphorbia heteradena Jaub root extract and evaluation of their stability. Ceramics International, 2015. 41(10): p. 14435-14439.

Rajkumar, S., et al., Performance of simple green synthesized Ag incorporated TiO2 nanoparticles based photoanodes by doctor-blade coating as working electrodes for dye sensitized solar cells. Progress in Organic Coatings, 2022. 164: p. 106697.

Agarwal, H., A. Nakara, and V.K. Shanmugam, Anti-inflammatory mechanism of various metal and metal oxide nanoparticles synthesized using plant extracts: A review. Biomed Pharmacother, 2019. 109: p. 2561-2572.

Subhapriya, S. and P. Gomathipriya, Green synthesis of titanium dioxide (TiO(2)) nanoparticles by Trigonella foenum-graecum extract and its antimicrobial properties. Microb Pathog, 2018. 116: p. 215-220.